ACS SENSORS

pubs.acs.org/acssensors
Article

Kinetic FRET Assay to Measure Binding-Induced Conformational Changes of Nucleic Acids

R. Anahi Higuera-Rodriguez,* Mareike C. De Pascali, Masood Aziz, Michael Sattler, Ulrich Rant, and Wolfgang Kaiser*

Cite This: *ACS Sens.* 2023, 8, 4597−4606
Read Online

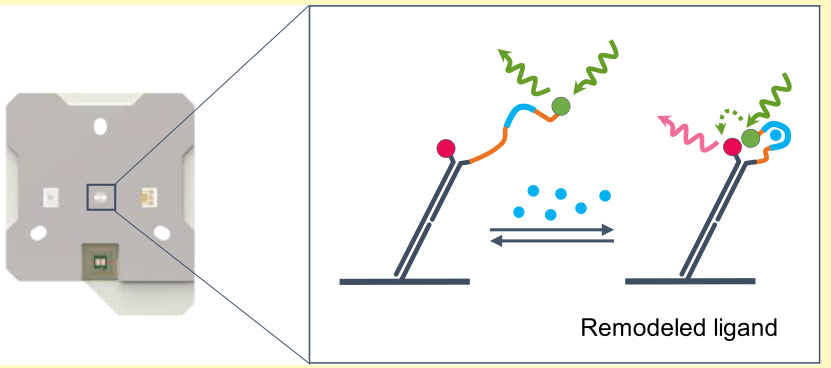

ABSTRACT: The interaction of small molecules or proteins with RNA or DNA often involves changes in the nucleic acid (NA) folding and structure. A biophysical characterization of these processes helps us to understand the underlying molecular mechanisms. Here, we propose kinFRET (kinetics Förster resonance energy transfer), a real-time ensemble FRET methodology to measure binding and folding kinetics. With kinFRET, the kinetics of conformational changes of NAs (DNA or RNA) upon analyte binding can be directly followed via a FRET signal using a chip-based biosensor. We demonstrate the utility of this approach with two representative examples. First, we monitored the conformational changes of different formats of an aptamer (MN19) upon interaction with small-molecule analytes. Second, we characterized the binding kinetics of RNA recognition by tandem K homology (KH) domains of the human insulin-like growth factor II mRNA-binding protein 3 (IMP3), which reveals distinct kinetic contributions of the two KH domains. Our data demonstrate that kinFRET is well suited to study the kinetics and conformational changes of NA−analyte interactions.

KEYWORDS: *biosensors, binding kinetics, Förster resonance energy transfer, nucleic acid conformational changes, aptamer, RNA binding protein, switchSENSE technology*

The time-dependency of binding events, i.e., binding kinetics, is a tool that enables a deeper characterization of dynamic systems compared to equilibrium studies. As binding at equilibrium can be the result of very different kinetic processes, binding kinetics are important for a better understanding of binding mechanisms and the development of small molecules[1] and biomolecule-based drugs.[2] Additionally, kinetic rates are directly connected to biomolecule functions within the cell.[3]

Förster resonance energy transfer (FRET)[4,5] is extensively used as a reporter technique in molecular biology due to its high sensitivity on the nanometer scale, which is relevant for interactions between biomolecules. The range of FRET-based assays can be divided into two main categories, ensemble and single-molecule FRET (smFRET). Ensemble FRET deals with an average of the molecules' conformations. Titration experiments are normally used to calculate FRET efficiency at equilibrium,[6−8] while time-resolved FRET (trFRET) is a combination of time-resolved fluorometry (TRF) and FRET.[9] A benefit of trFRET is that autofluorescent compounds can be used due to their shorter fluorescence lifetimes compared to the measured signal. Another advantage of trFRET compared to regular ensemble FRET is that not only the dissociation equilibrium constant (K_d) but also the association (k_{on}) and dissociation (k_{off}) rate constants can be extracted. However, these are indirectly calculated using linear regression of the observed rate ($k_{obs} = k_{on}[C] + k_{off}$). Therefore, rate constants determined with trFRET can be inaccurate, especially k_{off}

Received: July 25, 2023
Revised: October 27, 2023
Accepted: November 28, 2023
Published: December 7, 2023

https://doi.org/10.1021/acssensors.3c01527
ACS Sens. 2023, 8, 4597−4606

(intercept), which can be greatly affected by small changes in k_{on} (slope). Moreover, ensemble FRET—including trFRET—are mostly without flow, which means that the exchange of molecules to observe association and dissociation phases separately is not possible. Additionally, special fluorophores with high photostability or/and long emission lifetimes are required.

smFRET is typically performed on fluorescence microscopes and allows the study of individual molecules. These can be analyzed as individual populations in a heterogeneous sample, in contrast to ensemble FRET, which is an average of the whole population. Even though smFRET is a powerful technique to study the dynamics of small populations,[10,11] it requires a complex data analysis[12,13] and considerable experimental effort to characterize either very fast or slow interactions.[14,15]

On the other side, a standard technology used to measure the kinetics of solute analytes binding to surface-immobilized ligands is SPR (surface plasmon resonance). However, while FRET is a highly sensitive method to detect conformational changes in biomolecules, SPR measures the mean refractive index of the adsorbed biolayer. Structural changes may not be detectable by SPR or result in noninterpretable signals.

Here, we present a new technique: kinFRET, or kinetics FRET. kinFRET enables the investigation of the ensemble conformational change kinetics of nucleic acids (NAs) during a binding event. kinFRET is based on the switchSENSE biosensing technology,[16] which employs fluorescently labeled surface-immobilized DNA linkers to monitor the binding interactions of a variety of biomolecules.[17−19] The system uses a time-resolved single-photon counting detection setup and an epi-fluorescence microscope. The fluorescence signals depend on static quenching and/or dynamic quenching, also called collisional quenching. These two phenomena lead to a nonradiative energy transfer from the dye to the quencher[20−22] and a unique quenching or antiquenching profile upon analyte binding, which is referred to as the fluorescence proximity sensing (FPS) signal. Noteworthy features of the technique are the ability to discern the analyte−ligand complex interactions (binding) using FPS[18,19] and NA conformational change kinetics, as well as the adaptability of the system and the ability to measure the association and dissociation rate constants directly, thanks to the applied flow.

To demonstrate the utility of kinFRET, we investigated two systems involving molecules that modify the conformation of NA and from which binding kinetics have not been explored before. The first example is the cocaine-binding aptamer.[23,24] The binding of molecule analytes to this aptamer has been studied before and the aptamer has been optimized and diversified.[25,26] Advantages of short aptamers include high specificity, stability, and low production costs, which make them appealing for various applications, including their potential as alternative antibiotics.[27,28] The aptamer used in this work was originally evolved to specifically recognize cocaine,[29] but Reinstein et al. (2013)[25] found quinine to be an even stronger binder. From the previously reported aptamer variants in the literature, we selected the MN19 construct because of its flexible conformation to showcase the effortless detection of conformational changes with the kinFRET technique. The MN19 is a short aptamer (30 nt), providing a simple setup suitable to establish the technique and measure the kinetics of conformational changes via kinFRET. This aptamer is well studied and characterized[24−26,30−32] and served as a model system for kinFRET measurements.

Second, to showcase the capabilities of kinFRET, we studied a more complex and biologically relevant system, an oncofetal RNA binding protein (RBP): the human insulin-like growth factor 2 mRNA binding protein 3 (IMP3). IMP3 comprises two RNA recognition motifs and four K homology (KH) domains.[33,34] The KH domains are arranged and interact in tandem (KH1−2 and KH3−4) and have been shown to be key determinants binding to RNA.[35] A recent study demonstrated that IMP3 binds to clustered motifs composed of CA-rich regions and sequences with a CGGC core, specific to the KH2 and KH1 domains, respectively. The specific spacing between binding motifs is expected to lead to the formation of RNA loops when the protein binds.[36] It has been proposed that RNA-looping induced by protein binding assists the assembly of post-transcriptional regulatory elements by remodeling the transcript,[37,38] which can directly be related to how the protein stabilizes RNA within messenger ribonucleoprotein (mRNP) granules.[39] Here, we looked at the ability of IMP3 to loop RNA upon binding using RNA ligands present in the 3′ untranslated region of the key oncogenic mRNA transcript *ANKRD17*, which codes for a protein involved in cell cycle progression.[36,40] We focused on RNA remodeling by IMP3 KH domains 1 and 2 (KH1−2).

EXPERIMENTAL SECTION

NA Ligands. All NAs were chemically synthesized (Ella Biotech GmbH). Sequences can be found in Table S1. The ligands of interest were synthesized with a generic 48 nt DNA oligonucleotide (ligand strand, on the 3′ end of the ligand). This ligand strand is part of the DNA linker system on the heliX adapter chip (Dynamic Biosensors GmbH). The ligand strand was hybridized with the upper half of the adapter strand carrying a fluorophore (donor or acceptor) on its 3′ end. The lower half of the adapter strand is complementary to either spot 1- or 2-immobilized anchor strands on the chip surface (Figure 1). When a double-stranded ligand with an additional fluorescent dye was used, a short fluorescently labeled oligonucleotide, complementary to an extension of the ligand, was hybridized. Details on the hybridization are given in the Supporting Information experimental

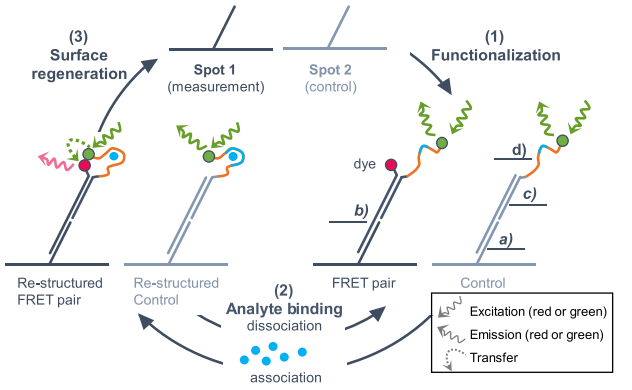

Figure 1. Standard workflow for kinFRET measurements. The symbols for excitation, emission, and energy transfer, described in the legend, are consistent with all the following figures. In phase 1, the ligands are immobilized on the chip surface. The second phase is the analyte binding phase, followed by buffer injection to start the dissociation step. The third phase (optional) is surface regeneration. The anchor strand (a) is fixed on the surface, while the prehybridized adapter strand (b) and ligand strand (c) with the DNA/RNA ligand overhang (d) are exchangeable.

https://doi.org/10.1021/acssensors.3c01527
ACS Sens. 2023, 8, 4597−4606

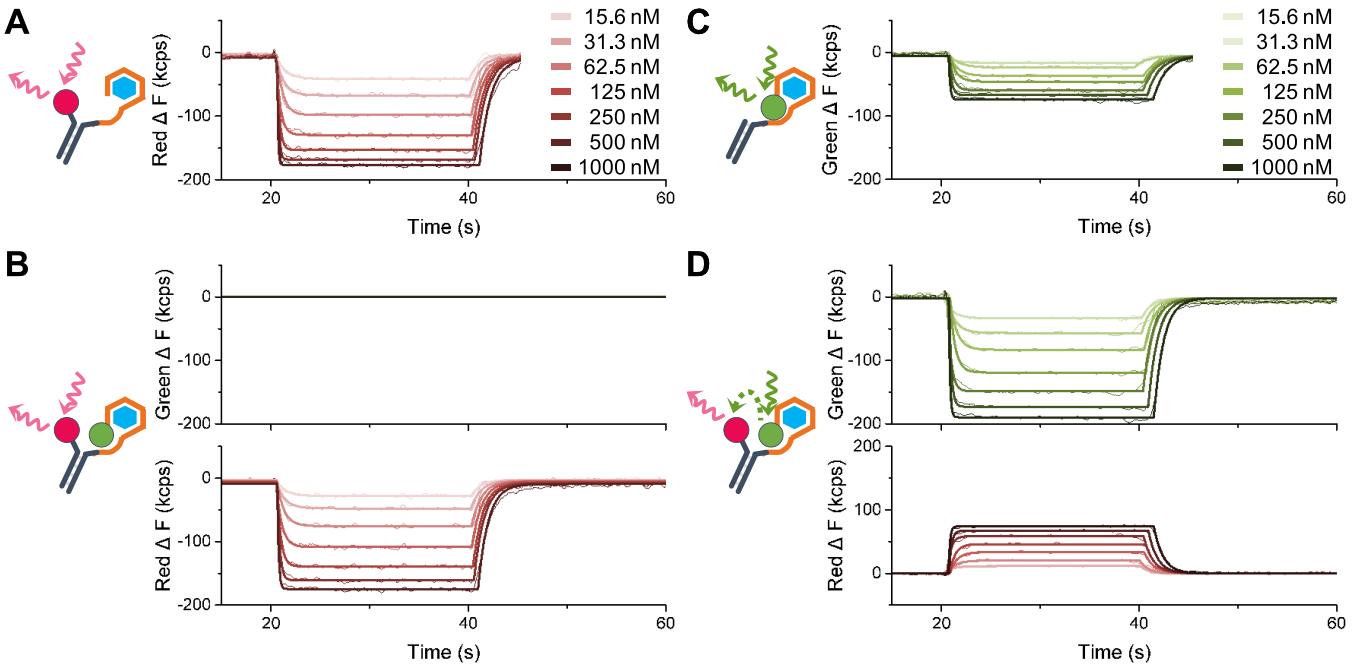

Figure 2. FPS and kinFRET measurements of the interaction between the MN19 aptamer with quinine. The excitation of the dyes during the measurement is schematically represented next to the traces. (A) Kinetic traces of the unmodified MN19 aptamer using the FPS mode with only the red fluorophore. (B) Detected red and green signals of the MN19-cov. aptamer using the FPS mode under red excitation. (C) FPS kinetics of the MN19-cov. aptamer in the presence of only the excited green dye. (D) kinFRET red and green signals detected with the MN19-cov. aptamer under green excitation.

section. Then, the strands were mixed in a 1:1 v/v ratio of adapters 1 and 2 and placed in the heliX$^+$ biosensor device. The functionalization of the chip was achieved by using standard procedures on the heliX$^+$ biosensor platform (hybridization for 200 s). The used red and green fluorescent dyes were chosen to form a FRET pair. Here, red fluorophores type a and b (Ra rhodamine derivative and Rb oxazine derivative) and a green fluorophore type a (Ga rhodamine derivative) were used from Dynamic Biosensors GmbH, but any FRET dye pair could be potentially used for this method (see Figure S1 for details on the optical filters).

kinFRET Experiments. kinFRET experiments were performed using switchSENSE proximity sensing technology[41,42] and a heliX adapter chip on the heliX$^+$ biosensor platform (Dynamic Biosensors GmbH). The optoelectronic and fluidic handling schematic can be seen in Figure S1 and additional technical details in the Supporting Information experimental section.

Only the donor is excited during the kinFRET experiments if not stated otherwise. The workflow of kinFRET measurements is depicted in Figure 1. The first step is the functionalization of the surface with the prehybridized adapter-ligand strand complex carrying the target sequence. In the second step, the association phase starts when the analyte is injected into the chip with constant flow, while the dissociation phase is marked by the exchange of the analyte solution with buffer at constant flow. In the last step, the surface is regenerated. Details on the kinetic traces data treatment and NA secondary structure predictions can be found in the Supporting Information experimental section. All experiments were performed at 25 °C.

kinFRET Experiments of the Aptamer. Quinine hemisulfate salt monohydrate (Sigma), amodiaquine dihydrochloride dihydrate (Sigma), and chloroquine diphosphate salt (Sigma) were diluted in TE140 running buffer (10 mM Tris−HCl, 140 mM NaCl, 0.05% Tween20, 50 μM EDTA, 50 μM EGTA, pH 7.4). The flow rate for the association of analyte was 200 μL/min for 20 s and 500 μL/min during 60 s long dissociation, with a sampling rate of 20 Hz. No regeneration of the surface was required due to the complete dissociation of the analyte.

Single Color Kinetics of the Aptamer. Kinetics experiments with one fluorescent dye were carried out the same way as kinFRET experiments, with the difference that only the red or green fluorophore was excited.

kinFRET Experiments of IMP3-RNA Binding. Details of protein expression and purification, as well as circular dichroism of the RNA ligand, can be found in the Supporting Information experimental section. Prior to kinFRET experiments, proteins were dialyzed in PE140 buffer (10 mM Na_2HPO_4/NaH_2PO_4, 140 mM NaCl, 0.05% Tween20, 50 μM EDTA, 50 μM EGTA, pH 7.4), which was used as the running buffer. To ensure protein stability, 1 mM TCEP was added to the buffer used for dilutions. The duration of the association and dissociation phases was 9 and 45 min, respectively, with a flow rate of 50 μL/min and a sampling rate of 1 Hz. A surface regeneration step was performed after every protein concentration was measured.

RESULTS AND DISCUSSION

Single Dye Kinetics Show Fast Interaction of Quinine with an Aptamer. To gain an understanding of the system, we first focused on the kinetics of quinine toward the MN19 aptamer using the FPS mode with a single red dye and then compared the single dye kinetics with kinetics in the kinFRET mode. The kinetic profile in Figure 2A shows a concentration-dependent signal change, where the association of quinine leads to a quenching of the fluorescent signal and dissociation restores the initial fluorescence by reaching equilibrium very quickly. The formation of the analyte−ligand complex, and even the sole presence of the ligand near the fluorophore, affects the dye through static and dynamic fluorescence quenching.[8]

The FPS signal of the red dye monitors a combined signal of binding and conformational change kinetics without discrimination between the two processes. Quinine is known to have a strong affinity to the aptamer.[25] To determine the association rate constant k_{on}, the dissociation rate constant k_{off}, and the dissociation equilibrium constant K_d, the kinetic traces can be

https://doi.org/10.1021/acssensors.3c01527
ACS Sens. 2023, 8, 4597−4606

fitted with a global monoexponential model (for results, see Table S2 and Equations S1).

Aptamer−Quinine Interaction Can Be Measured in Kinetics FRET Mode. To investigate the binding mechanism in more detail, we developed a kinFRET measurement setup with an additional green dye as a donor to form the FRET pair. For these measurements, we covalently attached a green dye to the 5′ end of the aptamer, which is referred to as MN19-covalent (MN19-cov.).

This setup was measured first by exciting only the red dye (Figure 2B) to characterize the modified aptamer and ensure that the additional green dye has no influence on the ability to monitor binding via red fluorescence. Due to the lack of green excitation, no change in green fluorescence is observed. In contrast to this, the red FPS signal shows a quinine-dependent decrease upon association. The signal change is very alike to the nonmodified MN19 aptamer (Figure 2A) with a similar change in amplitude, which indicates that the attached green dye does not affect the capability of the red dye to measure this interaction. Then we analyzed the signal reported from the attached green dye, in the absence of the red dye (Figure 2C). Different concentrations of quinine lead to a concentration-dependent quenching of the dye, suggesting that the covalently attached green dye can also sense the interaction with quinine. Lastly, we looked at the complete FRET setup, in which both donor green dye and acceptor red dye were present under green excitation (Figure 2D). Upon the injection of quinine, there is a concentration-dependent decrease in the green fluorescent signal, while the red fluorescent signal increases. When dissociating the analyte, the initial fluorescence is restored quickly. The green dye decreases in fluorescence not only because of the energy transfer to the red dye (FRET) but also due to the binding interaction itself and the folding when the dye comes close to the terminal bases of the adapter strand (FPS signal), as was shown in Figure 2C.

We initially exemplified the use of a covalently attached dye to form the FRET pair. However, for other applications with more complex ligands (e.g., long RNA ligands, as in the example of the IMP3 RBP, see below), an indirect (and exchangeable) attachment of the dyes is advantageous. Such an aptamer design is referred to as MN19-exchangeable (MN19-exch.) and shows the indirect attachment of an additional dye with its complementary sequence bearing a green donor dye.

The kinFRET signal, i.e., the increase in red fluorescence due to a conformational change of the DNA was observed for MN19-exch.,which exhibited similar signals as those of MN19-cov. (Figure S2A,B).

Conformational Changes of an Aptamer upon Analyte Binding Observed by kinFRET. To understand the signal changes observed during kinFRET measurements for both MN19-cov. and MN19-elong., we refer to the secondary structure prediction of the free form of the aptamer, depicted in Figure S3. The prediction shows two stem-loops and open 3′ and 5′ ends. The maximum calculated distance[43] of the terminal bases is 10.3 nm for MN19-cov. and MN19-elong., including the two additional thymines as spacers before the green dye. This is the upper limit at which FRET transfer can happen. When associating quinine to the aptamer, the signal change can be explained by a conformational rearrangement of the partially folded aptamer, where quinine stabilizes a more closed conformation bringing the terminal ends of the aptamer closer and, with this, the donor dye closer to the acceptor, where the secondary structure can be found in the literature.[25,26,31]

Aptamer Modifications and Different Small-Molecule Analytes Lead to Distinct Kinetic Processes. All kinetic traces of quinine-induced folding can be fitted with a global monoexponential fit model to get k_{on} and k_{off} (Table S2 and Equations S1). These are shown in the rate-scale plot (Figure 3) and discussed in the following section, where only the

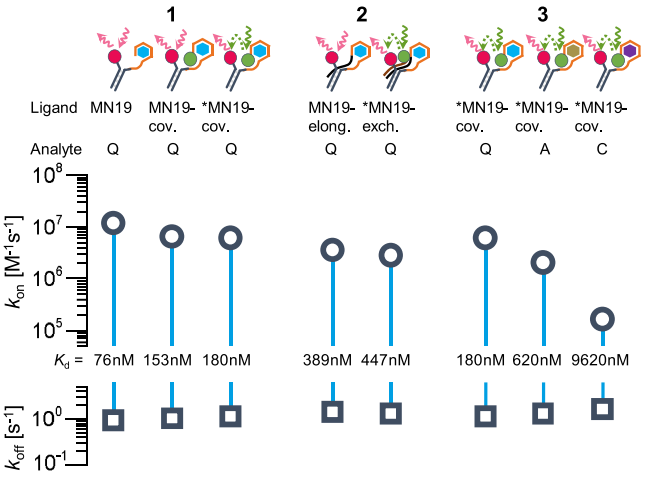

Figure 3. Kinetic rate constant overview of the aptamer interacting with small molecules. All measured kinetics between the different aptamer constructs interacting with small molecules [quinine (Q), amodiaquine (A), or chloroquine (C)] as analytes were fitted with a global monoexponential fitting model. Shown here are the rates of the red signal plotted in a rate-scale plot. The respective errors can be found in Table S2. The excitation channel is indicated by colored arrows, and the asterisk marks the ligands that are measured in kinFRET mode.

detected red signal is represented. To understand the kinetic traces, we compare different groups of measurements: first, the influence of an additional fluorescent dye and bases on the aptamer; second, the folding process in the presence of an elongated ligand; third, the comparison of FPS and kinFRET modes with respect to the conformational change; and fourth, the effect of different small molecules interacting with the aptamer.

The K_d is obtained by the ratio of k_{off} (s^{-1}) over k_{on} (M^{-1} s^{-1}). The first column in the rate-scale plot of Figure 3 shows the kinetics of quinine interacting with MN19 detected with a red dye on the adapter strand. Shown next to this is the MN19-cov. with two additional thymines and a green dye on the 5′ end, excited in red (FPS mode), and adjacent, the same setup can be seen excited in green (kinFRET mode). Note that in the FPS mode, we observe the conformational changes and the binding process in parallel, whereas the red signal from the MN19-cov. measured in the kinFRET mode report only on conformational changes. The k_{on} is around twofold lower for the MN19-cov. aptamers in both FPS and kinFRET mode compared to the nonmodified MN19 measured in FPS mode, resulting in the same increase of a factor of 2 for the K_d, since the k_{off} are virtually the same. The fact is that the k_{on} of the same MN19-cov. aptamer measured in FPS mode ($6.47 \pm 0.24 \times 10^6$ M^{-1} s^{-1}) and in kinFRET mode ($6.00 \pm 0.22 \times 10^6$ M^{-1} s^{-1}) is nearly the same, supporting our assumption that the decreased k_{on} compared to the nonmodified MN19 can be attributed to an increased hydrodynamic drag, which slows

https://doi.org/10.1021/acssensors.3c01527
ACS Sens. 2023, 8, 4597−4606

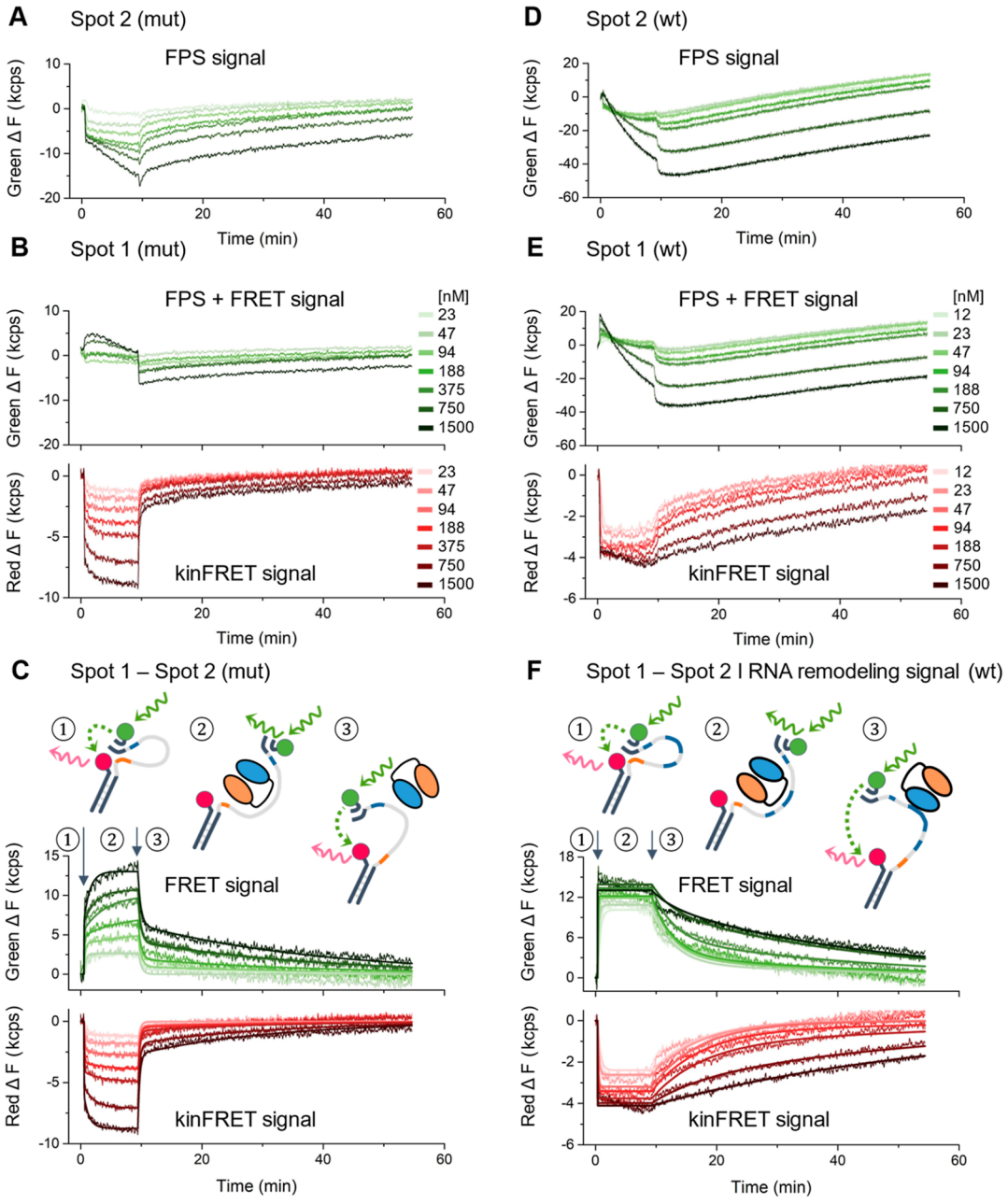

Figure 4. kinFRET measurements of IMP3 KH1−2 protein binding to RNA ligands with single or multiple binding motifs. For the mutant ligand, the signal recorded with the green dye on spot 2, reporting solely the FPS signal, is displayed in (A). The signal recorded with the donor dye and acceptor dye on spot 1 is shown in (B). The mirroring signals for green and red dyes after subtracting the green FPS signal of spot 2 from the green FPS + FRET of spot 1 are shown in (C). Here, the traces can be divided into three phases: 1, baseline displaying the initial RNA secondary structure in a FRET-sensitive distance; 2, protein binding and disrupting FRET; and 3, protein dissociation and restoring of FRET. The KH1 and its RNA motif are represented in orange, while KH2 with its RNA motif are in blue. A global biexponential fit was applied to the data (darker solid lines). The same process is shown in (D−F) for the wild-type ligand.

down the folding, caused by the additional dye together with two bases used as a spacer. From the literature, the K_d values of MN19 interacting with quinine determined with ITC are 0.23 ± 0.09 μM,[26] 0.4 ± 0.1 μM,[31] 0.7 ± 0.2 μM,[25] and 0.96 ± 0.04 μM,[32] while using electrochemical impedance spectroscopy (EIS), the K_d is 0.54 ± 0.02 μM.[32] Note that the values are diverse, even using the same methodology. Additionally, ITC and EIS rely on equilibrium measurements in which micro- to millimolar concentrations of the interacting partners were used. We determined the K_d using k_{on} and k_{off} as well as analyte concentrations spanning 2 orders of magnitude (15.6 nM^{-1} μM). This resulted in a K_d of 0.076 ± 0.003 μM.

Now we compare the MN19-elong. and MN19-exch. (Figure 3, middle panel) to examine the folding process in the presence of an elongated ligand. The interaction of quinine with the MN19-elong. construct (Figure S4) was measured only with the red dye in the FPS mode and compared with the MN19-exch. (Figure S2) measured in the kinFRET mode. This control experiment shows that the FPS mode as well as the kinFRET mode result in a similar K_d of 389 nM for MN19-elong. and 447 nM for MN19-exch. Even though the elongated

https://doi.org/10.1021/acssensors.3c01527
ACS Sens. 2023, 8, 4597−4606

overhang is nearly the same length as the aptamer itself (three nucleotides shorter), the k_{on} is affected only slightly. We attribute this small difference to the increased molecular weight and hereby to the increased hydrodynamic drag compared to the MN19-cov. which is not elongated. The influence of the hydrodynamic drag of an additional dye is more important for a shorter ligand than for a longer one since the relative increase is larger. A decreased k_{on} is expected as the k_{on} is affected by diffusion, long−range interactions, and conformational rearrangements of the ligand while forming the complex, which can be dependent on the length of the ligand itself. The k_{off} does not change and is mainly dependent on short-range interactions like hydrogen bonds and van der Waals interactions.[44] Nevertheless, the conformational changes seem to remain the same for all of the ligand variations.

To investigate if the binding of quinine and aptamer folding is a one- or a two-step process, we compared the measurements in the FPS (in which we cannot distinguish between binding and conformational changes) and the kinFRET mode (in which the red signal comes exclusively from a conformational change). Both signals result in equilibrium constants in the same range as those of MN19 and MN19-cov. differing by a factor of 2.3 and of MN19-elong. and MN19-exch. differing by a factor of 1.1. We already concluded that an additional dye leads to an increase in the hydrodynamic drag and therefore reduces the k_{on}. However, the affinities remain on the same order of magnitude. Therefore, we assume that both conformational change and binding events are equally fast and within the same time resolution limit. Consequently, both phenomena are observed as a one-step process. Our results are comparable with the results of Reinstein et al. (2013)[25] from NMR, ITC, and SAXS measurements, the latter showing differences in the pairwise density distribution functions (PDDF) plot between the free and quinine-bound MN19 aptamer forms. Other methods, such as ^{1}H NMR spectra,[45] EPR spectra,[46] and aptamer-based electrochemical biosensors,[47] have also confirmed a conformational change upon analyte binding to the aptamer.

Finally, we discuss different small-molecule analytes interacting with the same MN19-cov. aptamer (Figure 3, third column). The corresponding kinetic traces obtained in the kinFRET mode can be found in Figure S5A,B. Even though quinine, amodiaquine, and chloroquine share a structural similarity (Figure S6), the rates of the conformational change signal in red are quite different. The k_{off} values are again very similar, but the k_{on} values vary by a factor of ∼50 resulting in very different K_d values of 180 nM for quinine, 620 nM for amodiaquine, and 9620 nM for chloroquine. Weaker interactions led to an observable decrease in the closed conformation. Therefore, kinFRET allows a classification of small molecules based on conformational change signals. This is remarkable since, to our knowledge, the binding properties of these molecules have not been determined before with the MN19 aptamer.

Overall, we measured the conformational change kinetics of the aptamer using kinFRET. Different attachments of the dyes for kinFRET experiments result in a similar K_d, but more importantly, this shows that with flexible adjustments to various assay conditions, kinFRET can be applied in aptamer−small molecule conformational change screening.

Monitoring RNA Conformational Changes upon IMP3 Protein Binding. Now we focus on a different system involving protein−RNA interactions to demonstrate the adaptability of the kinFRET technique. We utilized kinFRET to characterize the RNA-remodeling properties of IMP3 KH1−2 with two *ANKRD17* mRNA-derived ligands. They are termed wild-type (wt) and mutant (mut). The predicted secondary structures, sequences for both ligands, and binding motifs are shown in Figure S7,B. The wt RNA ligand comprises multiple short-occurring RNA motifs including one motif for KH1 (CGGC) and four for KH2 (CACA/ACA) located on the 3′ and 5′ ends, respectively.[36] It must be noted that the presence of four KH2 motifs on the *ANKRD17* mRNA is not indicative of four KH2 domains binding to the respective motifs. But rather, the presence of those motifs enhances the local concentration of motifs in the vicinity of KH2 when binding as a tandem unit together with KH1. The binding of several KH2 domains on the many KH2 RNA motifs would be unlikely due to steric effects. The mut ligand has an altered nucleotide sequence from A8 to A25, which replaces those 18 nt with a poly-U RNA sequence.

This eliminates the three middle KH2 motifs and results in a ligand with one binding motif for KH1 and one binding motif for KH2. With this mutation, we wanted to assess the effect of motif multiplicity on the binding of IMP3 KH2, as well as on IMP3-induced remodeling and looping of the target RNA. Spot 1 was functionalized with the ligand and with both donor (green) and acceptor (red) dyes, while the second spot carried only the donor dye. For the donor dye, spot 1 records a mix of FPS and FRET signals, while spot 2 only records the FPS signal. The FPS signal depicts a more complex signal that combines the effects of protein-induced fluorescence enhancement (PIFE) or quenching (PIFQ),[48,49] as well as conformational changes. The different green and red signals provide multidimensional information on the binding mechanism, which will be described in the following paragraphs.

For simplicity, we first analyzed the mut ligand (Figure S7A) with only one binding motif per KH domain. The FPS signal recorded with the green dye on spot 2 can be seen in Figure 4A. This signal records the protein−RNA binding, resulting in a quenching of the green dye. The second signal that we can rationalize in order of simplicity is the red signal on spot 1, shown in the bottom red graph of Figure 4B. This signal change denotes that the acceptor is excited due to proximity to the illuminated green dye (<10 nm), which transfers its energy via FRET. Additionally, we see that the acceptor fluorescence decreases upon protein association and recovers during protein dissociation. This indicates that the initial state of the system is in a FRET-sensitive position and that the protein binding separates the dyes and results in a decreased FRET signal. Such a signal is referred to as the kinFRET signal. From this, we can conclude that the protein binding leads to a remodeling of the RNA ligand that separates the dyes that were initially in closer spatial proximity. Next, we focus on the green signal on spot 1, shown in the upper green graph of Figure 4B. The signal does not show saturation, and there is no clear exponential trend. This complex behavior is expected because the change in the fluorescence of the green dye is the sum of FRET (RNA conformational changes), as well as the FPS (PIFE and/or PIFQ) signal. We can deconvolute this complex signal by subtracting the FPS signal (data from Figure 4B) from the green dye signal in spot 2 (data from Figure 4A). The result represents the donor FRET signal due to the RNA conformational change, shown in the top green graph in Figure 4C, which mirrors the red signal in the plot underneath, as expected. This is confirmed by the similarity of the K_d obtained

https://doi.org/10.1021/acssensors.3c01527
ACS Sens. 2023, 8, 4597−4606

for the acceptor and donor signals for both the mut ligand (ca. 1.7-fold difference for the fast interaction and 1.1-fold difference for the slow interaction) and the wt ligand (ca. 2.6-fold difference for the fast interaction and 2.2-fold difference for the slow interaction).

Three phases can be observed within the traces in Figure 4C. The first one represents the initial state of the ligand enabling FRET. The secondary structure prediction of both RNA ligands, displayed in Figure S7A,B, suggests the formation of a loop by base paring of G1−C2−C3, where C3 is the first nucleotide within the KH2 CACA binding motif on the 5′ end, and C26−G27−G28−C29 from the KH1 CGGC binding motif close to the 3′ end. The predictions show only one, or sometimes a few, of many possible conformations of the RNA, and therefore, they must be interpreted with caution. A more realistic picture is that a dynamic equilibrium is present in the ensemble of molecules, in which the majority of RNA ligands adopt a conformation in a way that positions the red and green dyes in close proximity so that FRET can take place in the absence of the protein.

To confirm that the initial equilibrium ensemble of conformations of the ligand may exhibit intermolecular interactions, we determined the melting temperature to be 42 °C (Figure S8). The effects that contribute to stabilizing this equilibrium could include a lower entropic cost of a nonextended linear conformation,[50] intramolecular base pairing, a high local concentration of the complementary "sticky" ends, and the three hydrogen bonds shared between cytosine and guanine. The second phase is protein association, in which the dynamic equilibrium is shifted to a more open state of the RNA upon protein binding. As the domains interact with their corresponding motifs at the far opposing ends on the 3′ and 5′ ends for KH1 and KH2, respectively, FRET is reduced since the protein is looping the RNA and separating the dyes. The third phase is protein dissociation. As the domains separate from their motifs, the original secondary structure of the ligand is restored, along with FRET.

Multiple RNA Binding Motifs Lead to Strong Complex Formation with IMP3. The effect of multiple RNA motifs was addressed by kinFRET experiments of the protein toward the wt ligand comprising one binding motif for KH1 and four for KH2 (see Figure S7B). The analysis of the data is the same as that for the mut ligand. On spot 2, we can see the influence of the protein−ligand complex on the green dye resulting in the FPS signal (Figure 4D), while in spot 1, the green signal is a mixture between the FPS signal and the RNA conformational changes that separate the dyes upon binding, which decreases the FRET (Figure 4E, in green). For the acceptor dye, spot 1 directly shows the kinetics of RNA conformational changes (Figure 4E, in red).

When the FPS signal is referenced from spot 1 for the green signal, we obtain mirroring traces for donor and acceptor dyes that represent the RNA conformational change kinetics (Figure 4F).

The kinetics of the RNA conformational changes, i.e., the opening and closing of the secondary structure upon protein association and dissociation, were fitted to monoexponential and biexponential binding models for both ligands (mut and wt). The monoexponential model did not describe our experimental data well, as one can see in Figure S9A for mut and Figure S9B for wt ligands. In contrast, the biexponential model describes the experimental data better for both ligands (see Figure S9C for mut and Figure S9D for wt). The biexponential model incorporates two interactions with their corresponding k_{on1} and k_{on2}, k_{off1} and k_{off2}, and the calculated K_{d1} and K_{d2}, respectively. The kinetic rate constants and affinities are compared in Figure 5 and Table S3. We could

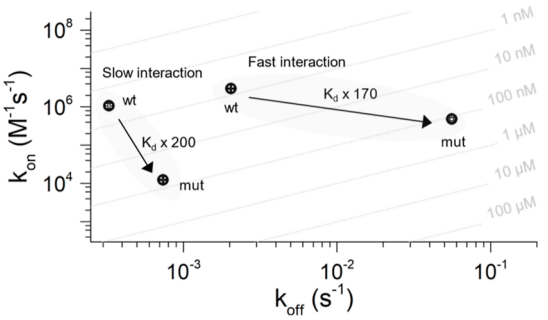

Figure 5. Comparison of conformational change kinetic rates of the wild-type (wt) and mutant (mut) ligands interacting with the IMP3 KH1−2 protein. A fast and a slow interaction were found for both mut and wt ligands. Data correspond to the acceptor signals for each ligand; error bars indicate the calculated error from the fit model.

identify two interactions for each ligand: one with faster association and dissociation rates and one with slower association and dissociation rates. For the mut ligand, the fast interaction has an approximately 39-fold faster association rate and a 76-fold faster dissociation rate compared to those of the slow interaction. For the wt ligand, the fast interaction has about a threefold faster association rate and a sixfold faster dissociation rate than the slow interaction. The difference between the slow and fast interactions indicates the strong cooperativity between protein domains to perform the RNA remodeling, in this case, the RNA looping. If we now compare the mut ligand with the wt ligand, the K_d shows an increase of about 170-fold and 200-fold for the fast and slow interactions, respectively. Regarding the slow interaction of both ligands, the nearly 90-fold increase in the k_{on} of the wt ligand compared to that of the mut ligand most likely reflects avidity due to the higher probability of the single KH2 domain encountering a (CACA/ACA) binding motif, given that there are four motifs present in the wt ligand compared to a single motif in the mut ligand. Concerning the fast interaction of both ligands, the ≈27-fold slower k_{off} of the wt ligand compared to that of the mut ligand is probably due to the stabilization effect that the multiple motifs for KH2 have on the binding of both protein domains. Taken together, we assume that the slow interaction reflects how KH2 recognizes multiple RNA motifs with avidity effects and potential effects on the RNA structure, while the fast interaction is a consequence of the KH1 interacting with its single RNA binding motif present in both ligands. Because not only the slow interaction (influenced by KH2 and its RNA motif multiplicity) but also the fast interaction (originating from KH1) is affected, we can conclude that there is a strong domain interplay between KH1 and KH2 in the tandem configuration. If the two KH domains would act as individual entities binding toward the RNA, one would expect that the fast interaction remains unchanged for both the wt and mut ligands, as both contain only one RNA binding motif for KH1. However, that is not the case, as we observe that the fast interaction strengthens its binding with the wt ligand mainly due to a slower k_{off}. This is attributed to the influence that the KH domains have on each other (cooperativity).

https://doi.org/10.1021/acssensors.3c01527
ACS Sens. 2023, 8, 4597−4606

Besides the change in the kinetic rates, there is a striking difference in the contribution of the slow and fast interactions to the closing of the RNA secondary structure during protein dissociation, which one can see in the dissociation traces in Figure 4C,F. For the mut ligand, the closing of the RNA back to its initial secondary structure is mainly due to the dissociation of the fast interaction, whereas for the wt, the dissociation of the slow interaction is rate-limiting. This indicates that the presence of four RNA binding motifs for KH2 in the wt ligand results in an increased local concentration and binding in multiple registers, which explains the reduced k_{off} indicating a higher protein−RNA complex stability for the wt compared to the mut ligand. Therefore, we assume that the slow interaction is the result of the KH2 domain binding to the multiple RNA motifs. Moreover, this increase in KH2-related complexes with RNA in the wt ligand is likely attributed to protein rebinding on the closely spaced motifs.

The kinFRET results suggest that the IMP3 protein can loop the RNA upon binding. Throughout this process, the protein can modify initial RNA secondary structures by shifting the RNA dynamic equilibrium toward a more open conformation. The kinetics data indicate that the fast interaction corresponds to the effect of the KH1 domain binding toward its motif and the slow interaction is the effect of the KH2 domain binding onto its RNA motif(s). The decrease of K_d, from the two-digit nanomolar for the mut ligand to the three-digit picomolar range for the wt ligand, indicates an increase in stability of the protein−RNA complex that loops the RNA as the KH2 motif number increases from 1 to 4, from the mut to wt ligand. Put together, along with the unlikeness that there are two or more proteins binding on the same RNA due to steric effects, we assume that KH2 rebinds to the closely spaced motifs on the wt ligand.

CONCLUSIONS

In this work, we demonstrated the potential of kinFRET ensemble measurements using the advantages of a biosensing platform−including the exchange of molecules with a constant flow and the wide range of affinities defined by the kinetic detection range of the heliX$^+$ biosensor itself (see the Supplementary experimental section)−to improve FRET measurements and easily extract real-time kinetics of NA conformational changes induced by analyte binding. The system is adaptable thanks to the straightforward surface functionalization and can be used to study a wide range of molecules including complex systems involving multiple binding pockets or multiple binding sites−−NAs interacting with small molecules, complementary sequences, and proteins. Additionally, the data treatment allows for the uncomplicated deconvolution of analyte-induced fluorescence change (FPS signal) and FRET signal by using two spatially separated measurement spots (under the same flow and detected simultaneously) with donor−acceptor dyes and only donor dye, respectively, on each spot.

The adaptability of the system is highlighted by the examples given in this work. In our first example, we investigated an aptamer interacting with quinine, amodiaquine, and chloroquine. By comparing the kinetics of quinine in FPS mode to the kinFRET experiments of the aptamer—both types of experiments within the same platform and the same chip type—we concluded that the binding and conformational change of the aptamer appear as a single process. We also tested a range of experimental setups in which the position and the attachment of the dyes varied, so that the experiment can be easily tailored to specific biomolecules. Additionally, slight changes in the chemical structures of the small molecules are resolvable with kinFRET and can be ranked. This "hit" ranking could accelerate drug discovery and development.

In our second example, we analyzed a very different system involving the IMP3 KH1−2 protein and the oncogenic mRNA *ANKRD17*. The protein can loop the RNA when binding to distant RNA motifs.[36−38] With kinFRET experiments, we were able to observe the looping process and RNA conformational changes in real time. Moreover, we observed that each KH domain contributes to this interaction with very different kinetic profiles. In addition, we compared the binding of the IMP3 protein toward one binding motif per domain (mut ligand) and one and four motifs for KH1 and KH2 (wt ligand), respectively. The results indicate that multiple motifs increase the protein−RNA complex stability, probably caused by rebinding. This added stability via multiple motifs could potentially be one of the mechanisms by which the protein stabilizes RNA within mRNP granules.

ASSOCIATED CONTENT

Supporting Information

The Supporting Information is available free of charge at https://pubs.acs.org/doi/10.1021/acssensors.3c01527.

Detailed information about oligonucleotide sequences, experimental setup, kinetic data treatment (including the fitting models used to describe kinetic data), secondary structure prediction of DNA and RNA ligands, kinetic constants and equilibrium constants of kinetics and kinetics FRET experiments for small molecule−aptamer interaction and for protein−RNA interaction, kinetics FRET traces for MN19 exch. aptamer construct, kinetic traces of MN19-elong. aptamer construct, kinetic traces of MN19-cov. aptamer construct interacting with small molecules, chemical structures of small molecules used to interact with aptamer, detailed information about protein expression and purification, circular-dichroism-derived plots for the *ANKRD17* ligand, and mono- and biexponential fits of kinetics FRET data of IMP3 protein (PDF)

AUTHOR INFORMATION

Corresponding Authors

R. Anahi Higuera-Rodriguez − *TUM School of Natural Sciences, Department of Bioscience, Technical University of Munich, Garching 85748, Germany; Dynamic Biosensors GmbH, Munich 81379, Germany;* orcid.org/0000-0002-4170-8799; Email: anahi.higuera@dynamic-biosensors.com

Wolfgang Kaiser − *Dynamic Biosensors GmbH, Munich 81379, Germany;* orcid.org/0000-0003-3578-504X; Email: info@dynamic-biosensors.com

Authors

Mareike C. De Pascali − *TUM School of Natural Sciences, Department of Bioscience, Technical University of Munich, Garching 85748, Germany; Dynamic Biosensors GmbH, Munich 81379, Germany*

Masood Aziz − *TUM School of Natural Sciences, Department of Bioscience, Technical University of Munich, Garching*

https://doi.org/10.1021/acssensors.3c01527
ACS Sens. 2023, 8, 4597−4606

85748, Germany; Helmholtz Munich, Molecular Targets and Therapeutics Center, Institute of Structural Biology, Neuherberg 85764, Germany; Present Address: Roche Diagnostics GmbH, 82377, Penzberg, Germany

Michael Sattler − *TUM School of Natural Sciences, Department of Bioscience, Technical University of Munich, Garching 85748, Germany; Helmholtz Munich, Molecular Targets and Therapeutics Center, Institute of Structural Biology, Neuherberg 85764, Germany*

Ulrich Rant − *Dynamic Biosensors GmbH, Munich 81379, Germany*

Complete contact information is available at: https://pubs.acs.org/10.1021/acssensors.3c01527

Author Contributions

R.A.H.-R. and M.C.D.P. contributed equally. All authors have given approval to the final version of the manuscript.

Funding

R.A.H.-R. acknowledges the funding received from the European Unionś Horizon 2020 research and innovation program under grant agreement no. 813239. M.S. acknowledges support by the German Research Foundation (DFG) grants SFB1309 (project no. 325871075), GRK1721 (project no. 178567888), and SPP1935 (project no. 273941853).

Notes

The authors declare the following competing financial interest(s): The authors R.A.H.R., M.C.P., M.A., U.R. and W.K. were employed by Dynamic Biosensors GmbH by the time the research was performed.

■ ACKNOWLEDGMENTS

We thank Hendrik V. Schröder for constructive discussions and inspiring ideas for the aptamer experiments, Adrian Walser for his help during data analysis, as well as Vivien Strauch for comments on the final draft of the manuscript.

■ ABBREVIATIONS

FRET, Förster resonance energy transfer; kinFRET, kinetics FRET; trFRET, time-resolved FRET; smFRET, single-molecule FRET; k_{on}, association rate constant; k_{off}, dissociation rate constant; K_d, equilibrium dissociation constant; NA, nucleic acid; RBP, RNA binding protein; mRNP, RNA within messenger ribonucleoprotein; KH, K homology; FPS, fluorescence proximity sensing; PIFE, protein-induced fluorescence enhancement; PIFQ, protein-induced fluorescence quenching; mut, mutant; wt, wild-type; IMP3, human insulin-like growth factor 2 mRNA binding protein 3

■ REFERENCES

(1) Ferruz, N.; De Fabritiis, G. Binding Kinetics in Drug Discovery. *Mol. Inf.* **2016**, *35*, 216−226.

(2) Mak, S.; Marszal, A.; Matscheko, N.; Rant, U. Kinetic analysis of ternary and binary binding modes of the bispecific antibody emicizumab. *mAbs* **2023**, *15*, 2149053.

(3) Sharma, D.; Zagore, L. L.; Brister, M. M.; Ye, X.; Crespo-Hernández, C. E.; Licatalosi, D. D.; Jankowsky, E. The kinetic landscape of an RNA-binding protein in cells. *Nature* **2021**, *591*, 152−156.

(4) Forster, T. Energiewanderung und Fluoreszenz. *Naturwissenschaften* **1946**, *33*, 166−175.

(5) Förster, T. Zwischenmolekulare Energiewanderung und Fluoreszenz. *Ann. Phys.* **1948**, *437*, 55−75.

(6) Lee, W.; Gillies, J. P.; Jose, D.; Israels, B. A.; von Hippel, P. H.; Marcus, A. H. Single-molecule FRET studies of the cooperative and non-cooperative binding kinetics of the bacteriophage T4 single-stranded DNA binding protein (gp32) to ssDNA lattices at replication fork junctions. *Nucleic Acids Res.* **2016**, *44*, 10691−10710.

(7) Li, J. J.; Fang, X.; Schuster, S. M.; Tan, W. Molecular Beacons: A Novel Approach to Detect Protein - DNA Interactions. *Angew. Chem., Int. Ed.* **2000**, *39*, 1049−1052.

(8) Didenko, V. V. DNA Probes Using Fluorescence Resonance Energy Transfer (FRET): Designs and Applications. *Biotechniques* **2001**, *31*, 1106−1121.

(9) Lamichhane, R.; Daubner, G. M.; Thomas-Crusells, J.; Auweter, S. D.; Manatschal, C.; Austin, K. S.; Valniuk, O.; Allain, F. H. T.; Rueda, D. RNA looping by PTB: Evidence using FRET and NMR spectroscopy for a role in splicing repression. *Proc. Natl. Acad. Sci. U.S.A.* **2010**, *107*, 4105−4110.

(10) Agam, G.; Gebhardt, C.; Popara, M.; Mächtel, R.; Folz, J.; Ambrose, B.; Chamachi, N.; Chung, S. Y.; Craggs, T. D.; de Boer, M.; et al. Reliability and accuracy of single-molecule FRET studies for characterization of structural dynamics and distances in proteins. *Nat. Methods* **2023**, *20*, 523−535.

(11) Voith von Voithenberg, L.; Sánchez-Rico, C.; Kang, H. S.; Madl, T.; Zanier, K.; Barth, A.; Warner, L. R.; Sattler, M.; Lamb, D. C. Recognition of the 3′ splice site RNA by the U2AF heterodimer involves a dynamic population shift. *Proc. Natl. Acad. Sci. U.S.A.* **2016**, *113*, E7169−E7175.

(12) Götz, M.; Barth, A.; Bohr, S. S. R.; Börner, R.; Chen, J.; Cordes, T.; Erie, D. A.; Gebhardt, C.; Hadzic, M. C. A. S.; Hamilton, G. L.; et al. A blind benchmark of analysis tools to infer kinetic rate constants from single-molecule FRET trajectories. *Nat. Commun.* **2022**, *13*, 5402.

(13) Chung, H. S.; Gopich, I. v.; McHale, K.; Cellmer, T.; Louis, J. M.; Eaton, W. A. Extracting rate coefficients from single-molecule photon trajectories and FRET efficiency histograms for a fast-folding protein. *J. Phys. Chem. A* **2011**, *115*, 3642−3656.

(14) van Oijen, A. M. Single-molecule approaches to characterizing kinetics of biomolecular interactions. *Curr. Opin. Biotechnol.* **2011**, *22*, 75−80.

(15) Vermeer, B.; Schmid, S. Can DyeCycling break the photobleaching limit in single-molecule FRET? *Nano Res.* **2022**, *15*, 9818−9830.

(16) Langer, A.; Hampel, P. A.; Kaiser, W.; Knezevic, J.; Welte, T.; Villa, V.; Maruyama, M.; Svejda, M.; Jähner, S.; Fischer, F.; et al. Protein analysis by time-resolved measurements with an electro-switchable DNA chip. *Nat. Commun.* **2013**, *4*, 2099.

(17) Cléry, A.; Sohier, T. J. M.; Welte, T.; Langer, A.; Allain, F. H. T. switchSENSE: A new technology to study protein-RNA interactions. *Methods* **2017**, *118−119*, 137−145.

(18) Ponzo, I.; Möller, F. M.; Daub, H.; Matscheko, N. A DNA-based biosensor assay for the kinetic characterization of ion-dependent aptamer folding and protein binding. *Molecules* **2019**, *24*, 2877.

(19) Schulte, C.; Soldà, A.; Spänig, S.; Adams, N.; Bekić, I.; Streicher, W.; Heider, D.; Strasser, R.; Maric, H. M. Multivalent binding kinetics resolved by fluorescence proximity sensing. *Commun. Biol.* **2022**, *5*, 1070.

(20) Iwunze, M. O. Fluorescence quenching. *Spectroscopy* **2001**, *16*, 14−22.

(21) Lakowicz, J. R. *Principles of Fluorescence Spectroscopy*, 3rd ed. Springer: New York, NY, 2006.

(22) Doose, S.; Neuweiler, H.; Sauer, M. Fluorescence quenching by photoinduced electron transfer: A reporter for conformational dynamics of macromolecules. *ChemPhysChem* **2009**, *10*, 1389−1398.

(23) Stojanovic, M. N.; de Prada, P.; Landry, D. W. Fluorescent Sensors Based on Aptamer Self-Assembly. *J. Am. Chem. Soc.* **2000**, *122*, 11547−11548.

(24) Neves, M. A. D.; Reinstein, O.; Johnson, P. E. Defining a stem length-dependent binding mechanism for the cocaine-binding

aptamer. A combined NMR and calorimetry study. *Biochemistry* **2010**, *49*, 8478−8487.
(25) Reinstein, O.; Yoo, M.; Han, C.; Palmo, T.; Beckham, S. A.; Wilce, M. C. J.; Johnson, P. E. Quinine binding by the cocaine-binding aptamer. Thermodynamic and hydrodynamic analysis of high-affinity binding of an off-target ligand. *Biochemistry* **2013**, *52*, 8652−8662.
(26) Neves, M. A. D.; Shoara, A. A.; Reinstein, O.; Abbasi Borhani, O.; Martin, T. R.; Johnson, P. E. Optimizing Stem Length to Improve Ligand Selectivity in a Structure-Switching Cocaine-Binding Aptamer. *ACS Sens.* **2017**, *2*, 1539−1545.
(27) Wang, H.; Mann, P. A.; Xiao, L.; Gill, C.; Galgoci, A. M.; Howe, J. A.; Villafania, A.; Barbieri, C. M.; Malinverni, J. C.; Sher, X.; et al. Dual-Targeting Small-Molecule Inhibitors of the Staphylococcus aureus FMN Riboswitch Disrupt Riboflavin Homeostasis in an Infectious Setting. *Cell Chem. Biol.* **2017**, *24*, 576−588.e6.
(28) Howe, J. A.; Wang, H.; Fischmann, T. O.; Balibar, C. J.; Xiao, L.; Galgoci, A. M.; Malinverni, J. C.; Mayhood, T.; Villafania, A.; Nahvi, A.; et al. Selective small-molecule inhibition of an RNA structural element. *Nature* **2015**, *526*, 672−677.
(29) Ulrich, H.; Ippolito, J. E.; Pagán, O. R.; Eterovic, V. A.; Hann, R. M.; Shi, H.; Lis, J. T.; Eldefrawi, M. E.; Hess, G. P. In vitro selection of RNA molecules that displace cocaine from the membrane-bound nicotinic acetylcholine receptor. *Proc. Natl. Acad. Sci. U.S.A.* **1998**, *95*, 14051−14056.
(30) Churcher, Z. R.; Neves, M. A. D.; Hunter, H. N.; Johnson, P. E. Comparison of the free and ligand-bound imino hydrogen exchange rates for the cocaine-binding aptamer. *J. Biomol. NMR* **2017**, *68*, 33−39.
(31) Slavkovic, S.; Eisen, S. R.; Johnson, P. E. Designed Alteration of Binding Affinity in Structure-Switching Aptamers through the Use of Dangling Nucleotides. *Biochemistry* **2020**, *59*, 663−670.
(32) Rahbarimehr, E.; Chao, H. P.; Churcher, Z. R.; Slavkovic, S.; Kaiyum, Y. A.; Johnson, P. E.; Dauphin-Ducharme, P. Finding the Lost Dissociation Constant of Electrochemical Aptamer-Based Biosensors. *Anal. Chem.* **2023**, *95*, 2229−2237.
(33) Bell, J. L.; Wächter, K.; Mühleck, B.; Pazaitis, N.; Köhn, M.; Lederer, M.; Hüttelmaier, S. Insulin-like growth factor 2 mRNA-binding proteins (IGF2BPs): Post-transcriptional drivers of cancer progression? *Cell. Mol. Life Sci.* **2013**, *70*, 2657−2675.
(34) Huang, H.; Weng, H.; Sun, W.; Qin, X.; Shi, H.; Wu, H.; Zhao, B. S.; Mesquita, A.; Liu, C.; Yuan, C. L.; et al. Recognition of RNA N 6 -methyladenosine by IGF2BP proteins enhances mRNA stability and translation. *Nat. Cell Biol.* **2018**, *20*, 285−295.
(35) Farina, K. L.; Hüttelmaier, S.; Musunuru, K.; Darnell, R.; Singer, R. H. Two ZBP1 KH domains facilitate β-actin mRNA localization, granule formation, and cytoskeletal attachment. *J. Cell Biol.* **2003**, *160*, 77−87.
(36) Schneider, T.; Hung, L. H.; Aziz, M.; Wilmen, A.; Thaum, S.; Wagner, J.; Janowski, R.; Müller, S.; Schreiner, S.; Friedhoff, P.; et al. Combinatorial recognition of clustered RNA elements by the multidomain RNA-binding protein IMP3. *Nat. Commun.* **2019**, *10*, 2266.
(37) Chao, J. A.; Patskovsky, Y.; Patel, V.; Levy, M.; Almo, S. C.; Singer, R. H. ZBP1 recognition of β-actin zipcode induces RNA looping. *Genes Dev.* **2010**, *24*, 148−158.
(38) Dagil, R.; Ball, N. J.; Ogrodowicz, R. W.; Hobor, F.; Purkiss, A. G.; Kelly, G.; Martin, S. R.; Taylor, I. A.; Ramos, A. IMP1 KH1 and KH2 domains create a structural platform with unique RNA recognition and re-modelling properties. *Nucleic Acids Res.* **2019**, *47*, 4334−4348.
(39) Degrauwe, N.; Suvà, M. L.; Janiszewska, M.; Riggi, N.; Stamenkovic, I. Imps: An RNA-binding protein family that provides a link between stem cell maintenance in normal development and cancer. *Genes Dev.* **2016**, *30*, 2459−2474.
(40) Schneider, T.; Hung, L. H.; Schreiner, S.; Starke, S.; Eckhof, H.; Rossbach, O.; Reich, S.; Medenbach, J.; Bindereif, A. CircRNA-protein complexes: IMP3 protein component defines subfamily of circRNPs. *Sci. Rep.* **2016**, *6*, 31313−31411.
(41) Rant, U.; Arinaga, K.; Fujita, S.; Yokoyama, N.; Abstreiter, G.; Tornow, M. Dynamic electrical switching of DNA layers on a metal surface. *Nano Lett.* **2004**, *4*, 2441−2445.
(42) Kaiser, W.; Rant, U. Conformations of end-tethered DNA molecules on gold surfaces: Influences of applied electric potential, electrolyte screening, and temperature. *J. Am. Chem. Soc.* **2010**, *132*, 7935−7945.
(43) Ambia-Garrido, J.; Vainrub, A.; Pettitt, B. M. A model for structure and thermodynamics of ssDNA and dsDNA near a surface: A coarse grained approach. *Comput. Phys. Commun.* **2010**, *181*, 2001−2007.
(44) Schreiber, G.; Selzer, T.; Albeck, S. Rational design of faster associating and tighter binding protein complexes. *Nat. Struct. Biol.* **2000**, *7*, 537−541.
(45) Churcher, Z. R.; Garaev, D.; Hunter, H. N.; Johnson, P. E. Reduction in Dynamics of Base pair Opening upon Ligand Binding by the Cocaine-Binding Aptamer. *Biophys. J.* **2020**, *119*, 1147−1156.
(46) Cekan, P.; Jonsson, E. Ö.; Sigurdsson, S. T. Folding of the cocaine aptamer studied by EPR and fluorescence spectroscopies using the bifunctional spectroscopic probe Ç. *Nucleic Acids Res.* **2009**, *37*, 3990−3995.
(47) Dauphin-Ducharme, P.; Churcher, Z. R.; Shoara, A. A.; Rahbarimehr, E.; Slavkovic, S.; Fontaine, N.; Boisvert, O.; Johnson, P. E. Redox Reporter - Ligand Competition to Support Signaling in the Cocaine-Binding Electrochemical Aptamer-Based Biosensor. *Chem.—Eur. J.* **2023**, *29*, No. e202300618.
(48) Lerner, E.; Ploetz, E.; Hohlbein, J.; Cordes, T.; Weiss, S. A Quantitative Theoretical Framework for Protein-Induced Fluorescence Enhancement-Förster-Type Resonance Energy Transfer (PIFE-FRET). *J. Phys. Chem. B* **2016**, *120*, 6401−6410.
(49) Ploetz, E.; Lerner, E.; Husada, F.; Roelfs, M.; Chung, S.; Hohlbein, J.; Weiss, S.; Cordes, T. Förster resonance energy transfer and protein-induced fluorescence enhancement as synergetic multi-scale molecular rulers. *Sci. Rep.* **2016**, *6*, 33257.
(50) Vicens, Q.; Kieft, J. S. Thoughts on how to think (and talk) about RNA structure. *Proc. Natl. Acad. Sci. U.S.A.* **2022**, *119*, No. e2112677119.

https://doi.org/10.1021/acssensors.3c01527
ACS Sens. 2023, 8, 4597−4606